Microscopic dynamics of ultracold particles in a ring-cavity optical lattice

Wolfgang Niedenzu,[1] Rainer Schulze,[1,2] András Vukics,[1] and Helmut Ritsch[1,*]

[1]*Institut für Theoretische Physik, Universität Innsbruck, Technikerstraße 25, A-6020 Innsbruck, Austria*

[2]*Institut für Ionenphysik und Angewandte Physik, Universität Innsbruck, Technikerstraße 25, A-6020 Innsbruck, Austria*

(Received 9 July 2010; published 8 October 2010)

The quantum dynamics of particles optically trapped in a symmetrically pumped high-Q ring cavity exhibits much richer physics than for a standing-wave resonator. In addition to modifying the lattice depth, light scattering by the particles shifts and reshapes the trapping potential. We calculate the corresponding changes in tunneling amplitudes and damping by an effective bipotential (two-level) model for the particle motion. As a crude truncation of the Bose-Hubbard model, expansion to the lowest band decouples particle and field dynamics. Only including excitations to higher bands can capture this essential additional physics and correctly describe decoherence, damping, and long-range correlations of the particle dynamics. The validity limits of the analytic models are confirmed by quantum Monte Carlo wave-function simulations, which exhibit correlated particle-field quantum jumps as unambiguous quantum signature of the system dynamics.

DOI: 10.1103/PhysRevA.82.043605 PACS number(s): 03.75.Lm, 37.30.+i, 05.30.Jp, 37.10.Vz

I. INTRODUCTION

In the past decade the theoretical and experimental study of ultracold quantum gases in optical potentials has seen tremendous progress and growth [1–3]. Optical lattices generated by spatially periodic laser fields can be routinely loaded with atoms very close to $T = 0$ with different filling factors and including multiple species [4]. Using magnetic fields or extra lasers the local interactions between the particles can be controlled providing for a versatile test ground of many-particle quantum phenomena. In most of these cases the backaction of the particles on the trapping and control fields is so small that the forces are well described by prescribed external potentials. Nevertheless for large lattices this backaction cannot be ignored and couples particle and field dynamics [5]. This coupled dynamics gets a particularly important new dimension when the light fields generating the potentials are enclosed in optical resonators [6] and the field amplitudes thus constitute separate dynamical quantum variables. Following initial theoretical studies [7] recent experiments now opened this new dimension by loading Bose-Einstein condensates (BECs) into optical resonators of high finesse [8–10]. Due to the large number of atoms the so-called strong-coupling limit of cavity QED was surpassed by several orders of magnitude reaching new parameter regimes of cavity QED and nonlinear quantum dynamics [9,11,12].

From a theoretical point of view, a dynamic lattice potential with quantum properties creates a wealth of new phenomena like atom-field entanglement, long-range interactions, and phononlike excitations with controllable properties. In particular, if several field modes are involved as in a ring cavity, new phenomena related to long-range (phonon-type) interactions of solid-state physics should become accessible for thorough tests in cold-atom setups. As a striking example, translation invariance and momentum conservation of the combined atom-field system induce pair correlations in the momentum space of the particles. Similarly, even small momenta transferred from atoms to the field should lead to measurable optical phase shifts [13], which might give a direct handle to observe the onset of superfluidity of the atoms or construct ultrasensitive acceleration detectors with BECs.

Of course, these new quantum degrees of freedom strongly increase the mathematical complexity of the theoretical model. As a first consequence the fairly simple, and for free-space optical lattices very successful, description of the system properties in terms of a single-band Bose-Hubbard model [1] cannot be directly applied in the case of dynamic potentials of varying depth and position. For standing-wave cavities an effective description in terms of self-consistent effective parameters has already been developed [14–16]. It will be a central goal of this work to develop improved approximative model descriptions for ring resonators and to study the limits, where a generalized version of the Bose-Hubbard model can still be applied to understand key features of the underlying physics.

Initially, setups of atoms in ring cavities were mainly considered to generalize and test cavity cooling of a wide class of polarizable particles, where no alternative laser cooling schemes exist. A ring geometry offers a wider capture range, faster cooling times [6], as well as lower temperatures [17], including even the idea of stopping and cooling a fast molecular beam [18]. An ultimate goal here is the development of an all-optical route to a BEC of polarizable point objects replacing evaporative cooling by cavity cooling which involves no particle loss. More recently, an alternative research direction studies quantum dynamics of atomic ensembles of very low temperature stored within a ring-cavity optical lattice [19,20]. As discussed in early theoretical work [21,22], controlling phase and amplitude of both pump fields of the ring cavity, which was verified in various experiments [19,23], gives great flexibility in controlling position and depth of the generated optical potential as well as the mode properties of lattice beams [24]. In the limiting case of a single-side pump one also recovers the model of the collective atomic recoil laser (CARL) [25,26]. First experiments using a single-side pump were already performed [20]. So far, the theoretical descriptions of BECs in ring cavities were mainly based on a Gross-Pitaevskii description of the atoms [20,27,28]

*Helmut.Ritsch@uibk.ac.at

and a coherent-state approximation for the cavity modes.

As for ultracold atomic gases in general the theoretical focus now shifts toward new quantum phases of degenerate gases near $T = 0$ [7,14,15,29,30], where mean-field approximations have to be abandoned. Interestingly, for the case of a single-mode standing-wave cavity it was possible to derive an effective Bose-Hubbard-type model which still proved valid for a dynamical quantized field creating the optical potential. This could capture important aspects of the dynamics and predict surprising modifications of the corresponding phase diagram [14–16]. As expected this dynamics in general invokes particle-field entanglement and nonlinear optics as well [31,32]. Here we investigate in which cases an extension of the Bose-Hubbard model for a ring-resonator-generated optical lattice is feasible. This is complicated by the fact that not only the lattice depth but also the lattice position are now fluctuating quantum variables. Thus already the definition of the proper Wannier basis functions is hard.

The article is organized as follows: We start with a tutorial review of the classical point-particle motion in ring-cavity-generated optical potentials and the presentation of the general atom-field Hamiltonian in Sec. II. In the following Sec. III we concentrate on the weak-coupling case, where only a single or a few excitations are generated in the unpumped mode and adiabatic effective potentials for the atomic motion can be derived on elimination of the mode dynamics. Here the cavity dynamics modifies tunneling and induces damping of nonlocal coherence. Subsequently, in Sec. IV we set out to derive an effective Bose-Hubbard-type model. Interestingly we miss central physical effects if we use the standard single-band approximation. Actually, central properties of ring-resonator-generated lattices appear in a two-band expansion presented in Sec. IV C, where tunneling is accompanied by photon scattering and jumps to the higher band. Finally, in Sec. V we compare an effective multiband model with numerical simulations of the coupled atom-field dynamics in full momentum space.

II. ONE POLARIZABLE POINT PARTICLE IN A RING RESONATOR

Let us first exhibit some essential physical properties of particle motion in ring cavities by considering a single linearly polarizable point particle moving inside a symmetrically driven ring resonator, cf. Fig. 1. The two counterpropagating modes with wave number k are pumped with amplitudes $\eta_\pm$ and decay at a rate κ. The pump frequency is detuned by $\Delta_c = \omega_{\text{pump}} - \omega_{\text{cavity}}$ with respect to the bare cavity resonance. Symmetric pumping, i.e., $\eta_+ = \eta_-$, generates a standing-wave field with spatial dependence $\propto \cos(kx)$ in the empty cavity. The second orthogonal field mode with spatial dependence $\propto \sin(kx)$ thus will not be excited by the pump [13], but it still cannot be ignored for the dynamics. Note that physical differences between a standing-wave resonator and a ring resonator have been investigated before, e.g., in Ref. [33]. At this point for simplicity we assume sufficient transverse localization of the particle so we can restrict ourselves to an effective one-dimensional description along the resonator axis.

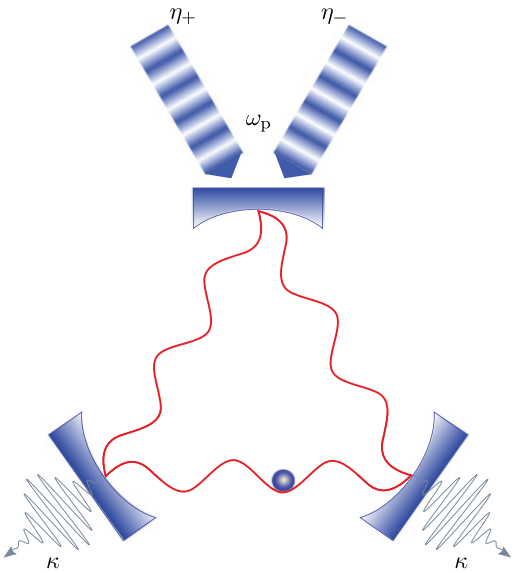

FIG. 1. (Color online) Sketch of the system: One polarizable particle in a symmetrically driven ring cavity (pumping fields η_+ and η_-). The resonator loss is characterized by the decay rate κ.

A. Classical and semiclassical description

Before turning to the quantum model we shall briefly review the corresponding classical field equations [6,22] to obtain a first qualitative insight into the underlying dynamical principles of the system. These classical equations of motion for the two driven and damped amplitudes of the counter-propagating modes coupled by a polarizable point particle read [22]

$$\dot{\alpha}_\pm = [i(\Delta_c - U_0) - \kappa - \Gamma_0]\alpha_\pm - (\Gamma_0 + iU_0)\alpha_\mp e^{\mp 2ikx} + \eta_\pm. \tag{1}$$

The central parameters U_0, which denotes the frequency shift of the mode induced by the particle, and Γ_0, which gives the particle-induced extra loss of the mode, are directly related to the real and imaginary parts of the particle's linear susceptibility [34,35]. These parameters also play a central role in the light forces determining the equations of motion for the particle [6]

$$F_{\text{dip}} = -4\hbar k U_0 \text{Im}(\alpha_+^* \alpha_- e^{-2ikx}), \tag{2a}$$

$$F_{\text{rp}} = 2\hbar k \Gamma_0 (|\alpha_+|^2 - |\alpha_-|^2), \tag{2b}$$

where (2a) is the dipole force and (2b) the radiation-pressure force. We see that U_0 gives the optical light shift and Γ_0 the photon scattering rate per photon in the mode. The dipole force can be derived from a potential proportional to the intracavity intensity and is—in a quantum picture—associated with the coherent redistribution of photons between the two modes. Depending on $\text{sgn}U_0$ the particles are trapped either at the intensity minima ($U_0 > 0$, "low-field seekers") or at the intensity maxima ($U_0 < 0$, "high-field seekers"). As we will focus on the dispersive, far-detuned limit where $\Gamma_0 \ll |U_0|$, we will neglect the radiation-pressure force (2b) and scattering loss in the following. Nevertheless, photons leak out of the resonator irreversibly and carry away momentum of the particle, which generates a nonconservative dynamics,

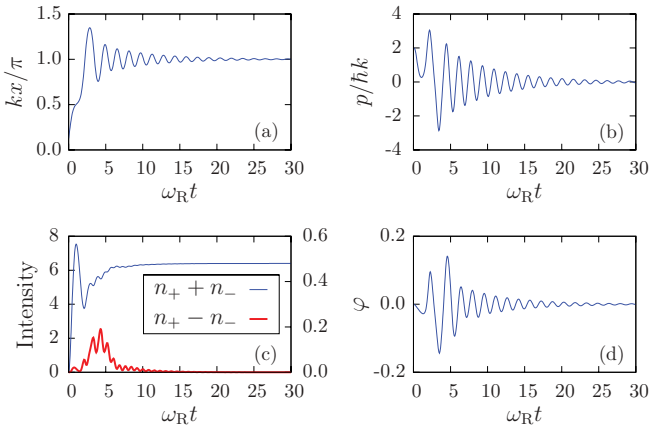

FIG. 2. (Color online) Particle motion in a ring cavity as solution of Eqs. (1) and (2). The particle moves along the cavity axis and eventually gets trapped. (a) Position, (b) momentum, (c) intensities split into symmetric (left y axis) and antisymmetric (right y axis) parts, and (d) phase shift from an initially $\cos^2(kx)$-shaped potential. Parameters: $\Delta_c = -2.6\omega_R$, $\kappa = \omega_R$, $U_0 = -0.3\omega_R$, and $\eta_+ = \eta_- = 4\omega_R$.

including friction and diffusion of particle motion [22]. The fluctuations in the photon numbers inducing diffusion (heating) then limit the final steady-state temperature [36] of the particle. Computation of this friction coefficient stemming from the dipole force indicates a cooling regime for $U_0 < 0$ and $\Delta_c < 0$ [6,22]. We will therefore concentrate on this parameter regime for the rest of this work.

We show a typical result of the combined particle-field equations in Fig. 2. An initially fast moving particle slows down while moving along the resonator axis before eventually getting trapped and oscillating around a potential minimum. This is reflected clearly in the field dynamics as well since symmetric pumping of the counterpropagating running waves corresponds to a pumped $[\propto \cos(kx)]$ and an unpumped $[\propto \sin(kx)]$ standing wave. A moving particle will scatter light from the cosine to the sine mode so that the resulting superimposed fields correspond to a shifted cosine mode. Hence also the resulting optical potential $[\propto \cos^2(kx)]$ gets shifted due to excitations of the sine mode as long as the particle moves. This can be clearly seen in Figs. 2(c) and 2(d). In the classical limit a particle at rest will scatter no more light into the sine mode and we obtain a pure cosine field in the resonator. In quantum mechanics the uncertainty relation will prevent this and quantum fluctuations of the particle position and momentum will couple the two modes even at zero temperature [17].

B. Quantum description

Let us now turn to a quantum description of the particle motion and the field modes. For convenience, we use a basis of $\{\cos(kx), \sin(kx)\}$ mode functions rather than the propagating wave modes $\{\exp(\pm ikx)\}$. This facilitates a straightforward comparison with the case of the standing-wave resonator by putting the coupling to the sine mode to zero and also allows for a better separation of the classical part of the field amplitude in the cosine mode. The corresponding Hamiltonian for symmetric pumping thus reads:

$$H = \frac{p^2}{2m} + \hbar U_0[a_c^\dagger a_c \cos^2(kx) + a_s^\dagger a_s \sin^2(kx)] + \frac{\hbar U_0}{2}(a_c^\dagger a_s + a_s^\dagger a_c)\sin(2kx) - \hbar\Delta_c(a_c^\dagger a_c + a_s^\dagger a_s) - i\hbar\eta_c(a_c - a_c^\dagger). \quad (3)$$

While the first line contains the optical potentials induced by the two field modes independently, the second line describes the particle-position-dependent coherent scattering of photons between the two modes. The third line contains the free-field evolution for both modes as well as the pumping of the cosine mode.

Let us first look at the corresponding Heisenberg equations for the particle momentum,

$$\dot{p} = \hbar k U_0(a_c^\dagger a_c - a_s^\dagger a_s)\sin(2kx) - \hbar k U_0(a_c^\dagger a_s + a_s^\dagger a_c)\cos(2kx), \quad (4a)$$

and for the mode amplitudes (dropping the input noise operators),

$$\dot{a}_c = \{i[\Delta_c - U_0\cos^2(kx)] - \kappa\}a_c - \frac{iU_0}{2}\sin(2kx)a_s + \eta_c, \quad (4b)$$

$$\dot{a}_s = \{i[\Delta_c - U_0\sin^2(kx)] - \kappa\}a_s - \frac{iU_0}{2}\sin(2kx)a_c. \quad (4c)$$

The first line of Eq. (4a) describes a force which solely depends on the photon numbers in the modes, whereas the second line is phase dependent and stems from the interference terms of the two modes of the intracavity electric field. In the special case of only one mode (e.g., setting $a_s = 0$) we recover the case of a standing-wave resonator. Small field amplitudes in the sine mode then simply induce a phase-dependent force on the particle while small deviations of the particle position from $x = 0$ determine the phase of the sine-mode field.

In the Schrödinger picture the time evolution of the density matrix ρ of the coupled system is determined by the master equation

$$\dot{\rho} = \frac{1}{i\hbar}[H,\rho] + \mathcal{L}_c\rho + \mathcal{L}_s\rho, \quad (5)$$

where the Liouvillean superoperator describing photon losses is given by [37]

$$\mathcal{L}_i\rho = \kappa(2a_i\rho a_i^\dagger - a_i^\dagger a_i\rho - \rho a_i^\dagger a_i),\ i \in \{c,s\}. \quad (6)$$

In general the field damping time will be shorter than the time scale of particle motion so the fields will reach a particle-dependent quasistationary state. For strong coherent pumping of the cosine mode one thus can approximate a_c by a coherent field of amplitude α_c and only treat the sine mode quantum mechanically. In the limit of very deep optical potentials, where particles are trapped near $x \approx 0$, this leads to the equations [17]

$$\dot{p} = 2\hbar k U_0(|\alpha_c|^2 - a_s^\dagger a_s)kx - \hbar k U_0(\alpha_c^* a_s + \alpha_c a_s^\dagger), \quad (7a)$$

$$\dot{a}_s = (i\Delta_c - \kappa)a_s - i\alpha_c U_0 kx, \quad (7b)$$

which are well known in optomechanics. In the opposite limit of a very weak potential and an initially flat particle distribution

($k = 0$) the $\sin(2kx)$ term will only amount to scattering to particle waves with $p = \pm 2\hbar k$ [38], where again a simple coupled-oscillator model can be applied. In this work we will concentrate on the general case where the particles are weakly trapped in the optical potential but still can tunnel between adjacent sites. This should finally lead to a Bose-Hubbard-type description with new types of long-range interactions.

III. EFFECTIVE POTENTIALS AND DYNAMICS IN THE WEAK-COUPLING LIMIT

As the general quantum dynamics is too complex for a direct solution we have to resort to interesting limiting cases. In this section we first work out the cavity-induced corrections to the particle dynamics in a classical potential. As outlined above the particles moving in the cavity field will scatter light between the modes and thus change the depth and shape of the optical potential. If the adjustment time of the field, i.e., the cavity decay, is faster than the typical particle motion, one can still expect to be able to define an effective potential for the particle. These cavity losses, from another viewpoint, can also be seen as a continuous measurement of the particle dynamics [39] which modifies the system dynamics via measurement backaction [40]. In the following we try to address these new key aspects in the strong-damping and weak-coupling limit, where they give only small corrections.

In a cavity the optical potential felt by the the particle is no longer conservative and constant as fluctuations in the field amplitude (quantum jumps) lead to momentum diffusion and dephasing of the wave function. This behavior is generic for a quantum system coupled to an open system. For free-space optical lattices the most important part of the decoherence stems from spontaneous photon scattering from the trap field to free space. However, for typical operating conditions far off any resonance, decoherence times are of the order of minutes rendering the light fields to constitute conservative classical potentials [2]. In a resonator-generated potential one has a second important contribution to decoherence via cavity decay. For sufficient atom-field coupling, the corresponding decoherence times can be quite short. Actually, one recovers the free-space conservative-field limit in the case of a very bad, "infinitely" fast decaying cavity together with a very strong pump and weak coupling, where the particles cannot induce any changes to the field dynamics.

In the following, we calculate corrections to this limit in the bad-cavity case via adiabatic elimination of the field dynamics. We first demonstrate semiclassically in secular approximation within the Schrödinger picture that the field always relaxes to a very low-excited state for properly chosen parameters. This allows us to derive an effective potential for the coherent particle dynamics. Still, the field dynamics induces dephasing as can be clearly observed on the decay of coherent tunneling oscillations due to photon scattering. In the following we will study this dephasing and derive an estimate for this decay rate.

A. Low-excitation limit in the Schrödinger picture

As seen from the Heisenberg equations (4) for the field modes the sine mode will only be populated by photons scattered in by the particles from the strongly pumped cosine mode. On the other hand, the driven cosine mode will be highly occupied and close to a coherent state $|\alpha_c\rangle$ with $|\alpha_c| \gg 1$. This generates an optical potential of depth $V_0 = \hbar|U_0||\alpha_c|^2$ forming a periodic optical lattice. In the limit of small $|\alpha_c||U_0|/|\Delta_c|$ we find only a very small field corresponding to at most one photon in the second mode. The wave function of the total system thus can be well approximated by the sum of a zero-photon and a one-photon component in the sine mode and a coherent state in the cosine mode. Neglecting higher sine-mode photon numbers as well as constant terms an effective approximate Hamiltonian in this limit thus can be conveniently written as

$$\begin{aligned} H = &\left(\frac{p^2}{2m} + \hbar U_0|\alpha_c|^2\cos^2(kx)\right) \\ &-\hbar[\Delta_c - U_0\sin^2(kx)]\tilde{\sigma}^+\tilde{\sigma}^- \\ &+\frac{\hbar U_0}{2}\sin(2kx)(\alpha_c^*\tilde{\sigma}^- + \alpha_c\tilde{\sigma}^+), \end{aligned} \tag{8}$$

where we have introduced the (photonic) raising and lowering operators $\tilde{\sigma}^+ := |1\rangle\langle 0|$ and $\tilde{\sigma}^- \equiv (\tilde{\sigma}^+)^\dagger = |0\rangle\langle 1|$. For simplicity and without loss of generality we choose the pump phase in a way that $\mathrm{Im}\,\alpha_c = 0$ in the following. The rather familiar-looking Hamiltonian (8) now exactly corresponds to a two-level particle moving in an optical potential, whose internal degrees of freedom are interacting with a classical spatially varying light field. Note that while the two states here physically describe zero or one photon in the sine mode and not actual internal particle excitations, the mathematics is the same as for an internal atomic excitation. Actually, in the past decades numerous ways to treat this generic laser-cooling Hamiltonian in different approximations have been developed.

Here we will follow the well-established *dressed-states* approach, based on the possibility to analytically diagonalize the Hamiltonian for any fixed-particle position x and determine the corresponding adiabatic field states. Hence x and p are treated as classical variables [41]. Alternatively, it would be also possible to directly solve the optical Bloch equations. Both methods start from a semiclassical approximation of the external particle variables. However, as shown in Refs. [42,43] there exists a corresponding consistent quantum-mechanical interpretation of the dressed-states picture. Here we will follow both approaches. The semiclassical approximation allows to obtain analytical results for the effective potential, which will give significant qualitative insight to the expected system dynamics and the latter treatment allows for an estimate of the effective motional decoherence and damping rates.

Diagonalization in the semiclassical limit yields the eigenvalues (the "adiabatic potentials" [44])

$$\begin{aligned} V_\pm(x) = &\hbar U_0\left(|\alpha_c|^2 - \frac{1}{2}\right)\cos^2(kx) \\ &-\frac{\hbar(\Delta_c - U_0)}{2} \pm \frac{\hbar\Omega(x)}{2} \end{aligned} \tag{9}$$

and the corresponding normalized eigenvectors

$$|x;+\rangle = \cos\vartheta\,|0\rangle + \sin\vartheta\,|1\rangle, \tag{10a}$$

$$|x;-\rangle = -\sin\vartheta\,|0\rangle + \cos\vartheta\,|1\rangle, \tag{10b}$$

where we have defined

$$\Delta(x) := \Delta_c - U_0 \sin^2(kx), \tag{11a}$$

$$\Omega(x) := \sqrt{\Delta^2(x) + U_0^2 |\alpha_c|^2 \sin^2(2kx)}, \tag{11b}$$

$$\sin\vartheta(x) := \mathrm{sgn}[U_0\alpha_c \sin(2kx)]\sqrt{\frac{\Omega(x)-\Delta(x)}{2\Omega(x)}}, \tag{11c}$$

$$\cos\vartheta(x) := \sqrt{\frac{\Omega(x)+\Delta(x)}{2\Omega(x)}}. \tag{11d}$$

For $|U_0||\alpha_c| \ll |\Delta_c|$ the state $|x;-\rangle$ contains only a very small amount of the one-photon state (it is thus a "quasidark state" [44]) since in leading order

$$\cos^2\vartheta(x) \simeq \frac{|\alpha_c|^2}{4}\frac{U_0^2}{\Delta_c^2}\sin^2(2kx), \tag{12a}$$

$$\sin^2\vartheta(x) \simeq 1 - \frac{|\alpha_c|^2}{4}\frac{U_0^2}{\Delta_c^2}\sin^2(2kx). \tag{12b}$$

The equations of motion for the two populations (in secular approximation which is valid for well-resolved lines, i.e., $\Omega(x) \gg \kappa \Rightarrow |\Delta_c| \gg \kappa$) read [41,45]

$$\dot{\Pi}_+ = -\Gamma_+^{\mathrm{eff}}\Pi_+ + \Gamma_-^{\mathrm{eff}}\Pi_-, \tag{13a}$$

$$\dot{\Pi}_- = -\Gamma_-^{\mathrm{eff}}\Pi_- + \Gamma_+^{\mathrm{eff}}\Pi_+, \tag{13b}$$

with the position-dependent effective rates

$$\Gamma_+^{\mathrm{eff}}(x) = 2\kappa \sin^4\vartheta(x), \tag{14a}$$

$$\Gamma_-^{\mathrm{eff}}(x) = 2\kappa \cos^4\vartheta(x). \tag{14b}$$

Its steady-state solution reads

$$\Pi_+ = \frac{\Gamma_-^{\mathrm{eff}}}{\Gamma_+^{\mathrm{eff}}+\Gamma_-^{\mathrm{eff}}} \simeq \frac{\Gamma_-^{\mathrm{eff}}}{\Gamma_+^{\mathrm{eff}}} = \left(\frac{\Omega+\Delta}{\Omega-\Delta}\right)^2, \tag{15a}$$

$$\Pi_- = \frac{\Gamma_+^{\mathrm{eff}}}{\Gamma_+^{\mathrm{eff}}+\Gamma_-^{\mathrm{eff}}} \simeq 1 - \frac{\Gamma_-^{\mathrm{eff}}}{\Gamma_+^{\mathrm{eff}}} = 1 - \left(\frac{\Omega+\Delta}{\Omega-\Delta}\right)^2. \tag{15b}$$

This state is reached within a time determined by the population decay rate $\Gamma_{\mathrm{pop}} = 2\kappa(\sin^4\vartheta + \cos^4\vartheta)$. Since $\Gamma_-^{\mathrm{eff}} \ll \Gamma_+^{\mathrm{eff}}$ the field will always end up in the local $|x;-\rangle$ state provided that $\omega_R \ll \Gamma_{\mathrm{pop}}$. The low-excitation approximation is thus well justified. For $U_0/\Delta_c \ll 1$ the steady-state populations (15) reduce to

$$\Pi_+ \simeq \frac{|\alpha_c|^4}{16}\frac{U_0^4}{\Delta_c^4}\sin^4(2kx), \tag{16a}$$

$$\Pi_- \simeq 1 - \frac{|\alpha_c|^4}{16}\frac{U_0^4}{\Delta_c^4}\sin^4(2kx). \tag{16b}$$

A small photon number in the sine mode is thus consistent with the approximation $\Pi_- \simeq 1$ as the photon number scales with U_0^2/Δ_c^2 and the population with U_0^4/Δ_c^4. Hence, in steady state the effective potential reads

$$\langle V(x)\rangle \simeq \hbar U_0 |\alpha_c|^2 \cos^2(kx) + \frac{|\alpha_c|^2}{4}\frac{\hbar U_0^2}{\Delta_c}\sin^2(2kx). \tag{17}$$

This is, of course, the same result as obtained for optical lattice potentials (ac Stark shift) [2]. There the potential is found to be $V(x) = \hbar|\Omega(x)|^2/4\delta$, where $\Omega(x)$ is the Rabi frequency and δ the detuning of the two-level system with respect to the driving laser. Setting $\Omega(x) := U_0\alpha_c \sin(2kx)$ and $\delta := \Delta_c$, the second part of equation (17) is recovered. The first part is just some additional classical potential which in our case does not affect the "internal" variables of the particle.

Let us now treat the problem in a closely related quantum-mechanical way. To this end we apply the unitary transformation

$$U = \begin{pmatrix} \cos\vartheta & \sin\vartheta \\ -\sin\vartheta & \cos\vartheta \end{pmatrix} \tag{18}$$

on the Hamiltonian (8). Assuming adiabaticity (nonadiabatic off-diagonal terms much smaller than the difference between the adiabatic eigenvalues [42]), the resulting Hamiltonian in the adiabatic basis $\{|+\rangle,|-\rangle\}$ reads [42]

$$H_{\mathrm{ad}} = \left[\frac{p^2}{2m} + \hbar U_0\left(|\alpha_c|^2 - \frac{1}{2}\right)\cos^2(kx)\right] + \frac{\hbar\Omega(x)}{2}(|+\rangle\langle+| - |-\rangle\langle-|). \tag{19}$$

The eigenstates of (19) are

$$|\Psi_{n,q}^{\pm}\rangle = |\phi_q^{n,\pm}\rangle|\pm\rangle, \tag{20}$$

where $|\phi_q^{n,\pm}\rangle$ denotes the Bloch state with quasimomentum q for the nth energy band of the two adiabatic potentials $V_\pm(x)$ defined in (9). Looking again at the rate equations stemming from the master equation, including photon decay, one finds the effective decay rates [46]

$$\Gamma_{n,q}^{+} = 2\kappa\langle\phi_q^{n,+}|\sin^2\vartheta|\phi_q^{n,+}\rangle, \tag{21a}$$

$$\Gamma_{n,q}^{-} = 2\kappa\langle\phi_q^{n,-}|\cos^2\vartheta|\phi_q^{n,-}\rangle. \tag{21b}$$

The dynamics described by the corresponding rate equations is shown in Fig. 3. Again, as in the semiclassical case we have $\Gamma_{n,q}^{+} \gg \Gamma_{n,q}^{-}$, and only the subspace belonging to $|-\rangle$ will be significantly populated in steady state. Therefore the adiabatic potential $V_-(x)$ can be treated as an effective potential for the particle motion as long as the incoherent processes within this subspace are sufficiently small [2]. Decoherence manifests itself as finite lifetime of the Bloch states within this potential, leading to a damping of the particle motion. This can be understood in the following way: Localized particles within the lattice are described by coherent superpositions of Bloch states [47]. If these coherences get lost due to a finite life time of the Bloch states, the particles can no longer coherently move through the lattice and experience an additional friction force. We estimate the effective rate to be

$$\Gamma \sim \max_q \Gamma_{0,q}^{-} \simeq 2\kappa\frac{|\alpha_c|^2U_0^2}{4\Delta_c^2}\max_q\langle\phi_q^0|\sin^2(2kx)|\phi_q^0\rangle, \tag{22}$$

which in a very crude approximation gives

$$\Gamma \lesssim 2\kappa\frac{|\alpha_c|^2U_0^2}{4\Delta_c^2} = \frac{|V_0|}{2}\frac{|U_0|\kappa}{\Delta_c^2}. \tag{23}$$

This rate has to be compared to the tunneling time T, which is determined by the inverse bandwidth of the lowest Bloch band. A high Q factor requires

$$\Gamma T \leqslant 2\kappa T\frac{|\alpha_c|^2U_0^2}{4\Delta_c^2} \overset{!}{\ll} 1. \tag{24}$$

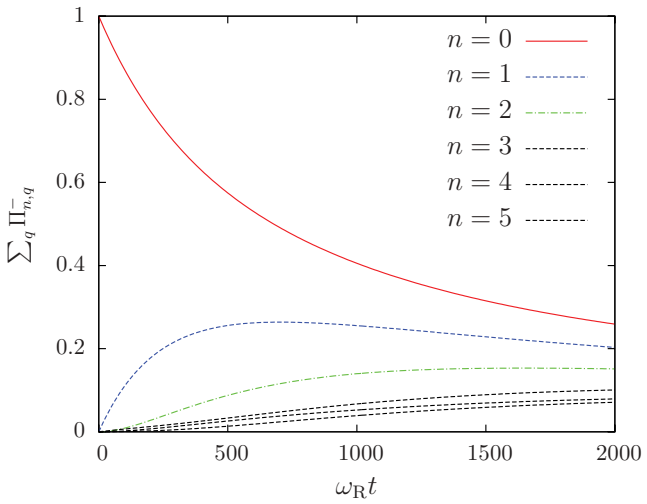

FIG. 3. (Color online) Time evolution of the band populations stemming from the rate equations in the basis (20) containing the rates (21). The potential depth is $V_0 = 25E_R$ and thus the first three bands are bound. Hence the lowest three curves ($n = 3, 4, 5$, from top to bottom) correspond to unbound states. We have assumed a double-well potential hence each band consists of two Bloch states with different quasimomenta. The initial state was $\Pi^-_{0,-1} = \Pi^-_{0,0} = 0.5$. There is no significant population transfer to the subspace belonging to the $|+\rangle$ adiabatic eigenstate, whereas the population distribution within the $|-\rangle$ subspace changes, the particle is heated. Parameters: $U_0 = -\omega_R$, $\alpha_c = 5$, $\Delta_c = -500\omega_R$, and $\kappa = 100\omega_R$.

B. Effective potential via adiabatic elimination in the Heisenberg picture

As a second alternative approach we will directly work in the Heisenberg picture. In contrast to the previous section, where we applied a two-level approximation for the field, we consider the full mode operator a here. Its equation of motion apart from the vacuum input noise operator reads

$$\dot{a} = [i\Delta(x) - \kappa]a - i\eta(x), \tag{25}$$

where we have defined

$$\eta(x) := \frac{\alpha_c U_0}{2} \sin(2kx). \tag{26}$$

Its formal steady-state solution reads

$$a = \frac{-i\eta(x)}{\kappa - i\Delta(x)}. \tag{27}$$

Hence one obtains the photon number

$$a^\dagger a = \frac{|\eta(x)|^2}{\kappa^2 + \Delta^2(x)} \simeq \frac{|\alpha_c|^2}{4} \frac{U_0^2}{\kappa^2 + \Delta_c^2} \sin^2(2kx), \tag{28}$$

where the latter is valid in the limit $U_0/\Delta_c \ll 1$. For $|\Delta_c| \gg \kappa$ it converges to the result (12a) obtained previously in the Schrödinger picture in secular approximation. The scattered coherent field $|\alpha(x)\rangle$ with amplitude (27) coincides with the steady-state solution $|x;-\rangle$ of the rate equations (13) in the same limit up to a phase depending on the (arbitrary) global phase of the eigenstates $|x;\pm\rangle$. Note that without the secular approximation κ also appears in the steady-state solution of the rate equations and thus in the photon number and the effective potential. The steady-state solution then can contain coherent superpositions of $|x;+\rangle$ and $|x;-\rangle$ as the states are not well enough separated.

The effective potential for the particle thus reads

$$\begin{aligned} V_{\text{eff}}(x) &= \hbar U_0 |\alpha_c|^2 \cos^2(kx) + \frac{\hbar\Delta(x)|\eta(x)|^2}{\kappa^2 + \Delta^2(x)} \\ &\simeq \hbar U_0 |\alpha_c|^2 \left[\cos^2(kx) + \frac{1}{4}\frac{\Delta_c U_0}{\Delta_c^2 + \kappa^2} \sin^2(2kx)\right], \end{aligned} \tag{29}$$

which equals the adiabatic potential $V_-(x)$ in the aforementioned approximation.

Now we can proceed exactly as before and estimate the particle's motion damping rate via the rates between the Bloch states,

$$\begin{aligned} \Gamma_{\text{eff}} &\sim \max_q 2\kappa \left\langle \phi_q^{0,\text{eff}} \left| \frac{|\eta(x)|^2}{\kappa^2 + \Delta^2(x)} \right| \phi_q^{0,\text{eff}} \right\rangle \\ &\simeq 2\kappa \frac{|\alpha_c|^2}{4} \frac{U_0^2}{\Delta_c^2 + \kappa^2} \max_q \langle \phi_q^{0,\text{eff}} | \sin^2(2kx) | \phi_q^{0,\text{eff}} \rangle. \end{aligned} \tag{30}$$

We have plotted this rate in Fig. 4 and the effective potential in Fig. 5. Figure 6 shows the particle motion for different parameters. The adiabatic elimination of the field dynamics results in a loss of information about the system and a broadening of the effective potential wells for the particles (cf. Fig. 5). Physically, this can be interpreted as a mixture of a shift of the cosine-squared potential to the left as well as to the right. These shifts originate from the single-photon field of undetermined phase in the sine mode. A similar situation occurs in transversally pumped standing-wave resonators [48], where for a given cavity-field phase every even potential well gets deepened (leading to self-organization of the particles) and for the opposite phase every odd well is deeper. After adiabatic elimination of the field the mixture of both effects can be observed which deepens the whole lattice. Note that the

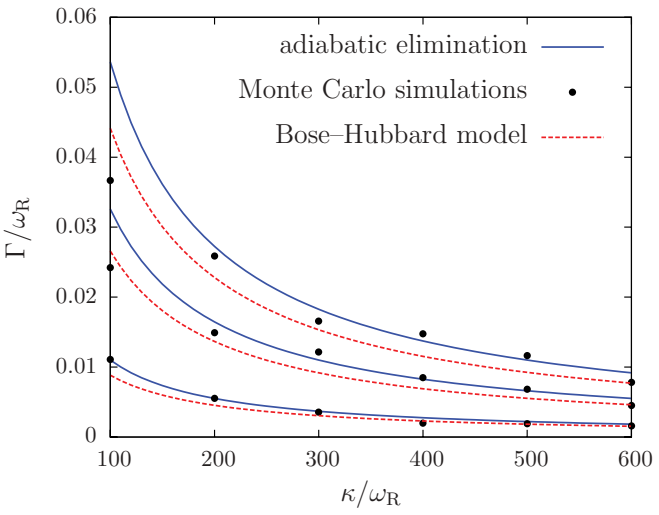

FIG. 4. (Color online) Damping coefficient Γ stemming from the adiabatic elimination (solid lines), from Monte Carlo wave-function (MWCF) simulations [dots, cf. Sec. V, model (ii)] and computed with the two-band Bose-Hubbard model (dashed lines) presented in Sec. IV C. The statistical error from the MCWFs is of the order of the point size. From bottom to top: $U_0 = (-1, -3, -5)\omega_R$. The other parameters are $\alpha_c = \sqrt{12\omega_R/|U_0|}$ and $\Delta_c = U_0 - \kappa$.

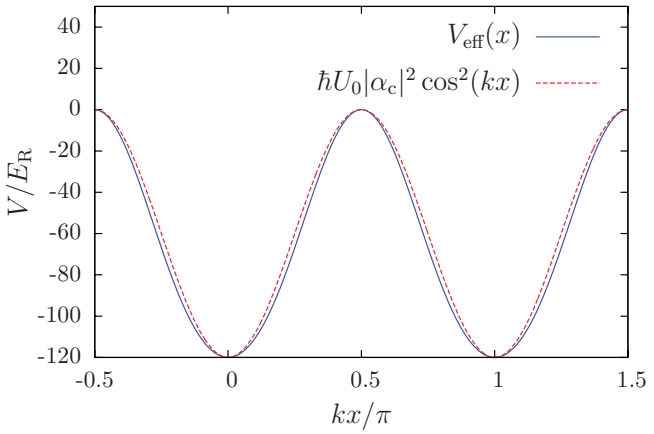

FIG. 5. (Color online) Effective potential $V_{\rm eff}(x)$ compared to the unperturbed potential $V(x)=\hbar U_0|\alpha_c|^2\cos^2(kx)$. At $kx=n\pi/2$ ($n\in\mathbb{Z}$) the two potentials agree as for these points the coupling to the mode vanishes. Parameters: $U_0=-50\omega_R$, $\alpha_c=\sqrt{2.4}$, $\Delta_c=-150\omega_R$, and $\kappa=100\omega_R$.

effect of different atoms in the same state adds up coherently here, so even a tiny single-particle effect could have dramatic consequences for a superfluid many-particle state in the lattice.

In principle the model could also be applied to the case of a BEC of N particles in the same motional state. In this case the backaction effect on the potential would be strongly enhanced and modifications of tunneling will lead to significant changes of the collective nonlinear dynamics of a corresponding mean-field model. We will, however, not pursue this route any further here and rather turn to a description in terms of localized basis function in the spirit of a Bose-Hubbard model.

IV. BOSE-HUBBARD MODEL FOR A RING-CAVITY POTENTIAL

The many-body version of the single-particle Hamiltonian (3) is conveniently obtained through a second-quantization formalism. With $\Psi(x)$ denoting the bosonic particle field operator, the corresponding Hamilton operator reads

$$H=\int dx\Psi^\dagger(x)H_1\Psi(x)-\hbar\Delta_c(a_c^\dagger a_c+a_s^\dagger a_s)-i\hbar\eta_c(a_c-a_c^\dagger)+\frac{g_{1D}}{2}\int dx\Psi^\dagger(x)\Psi^\dagger(x)\Psi(x)\Psi(x), \tag{31}$$

with

$$H_1=\frac{p^2}{2m}+\hbar U_0(a_c^\dagger a_c-a_s^\dagger a_s)\cos^2(kx)+\hbar U_0 a_s^\dagger a_s+\frac{\hbar U_0}{2}(a_c^\dagger a_s+a_s^\dagger a_c)\sin(2kx). \tag{32}$$

The two-body interaction at very low temperatures (s-wave scattering) is modeled by a short-range pseudopotential containing the scattering length [49]. As our central goal is to study the implications of the quantized potential, we will, however, neglect any direct particle-particle interaction for the moment. It can be reintroduced later by effective on-site interactions in the corresponding generalized Bose-Hubbard model.

In order to obtain a Bose-Hubbard description of the particle dynamics, the standard procedure is to expand

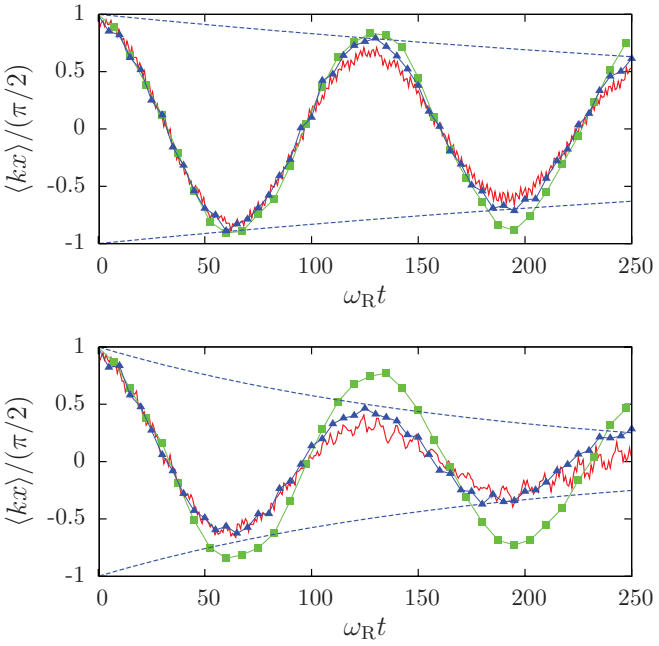

FIG. 6. (Color online) Particle motion simulated with three different models [cf. models (i)–(iii) in Sec. V]. [Red (solid line without additional points)] Solution of the complete ring resonator with both dynamical modes. [Green (squares)] Solution setting the coupling to the unpumped mode to zero, i.e., a standing-wave lattice formed by the pumped mode. [Blue (triangles)] Solution of the model (8), where the pumped mode has been set to a static coherent state. The blue (dashed) envelope is the exponential decay predicted in Eq. (30). As the photon number in the pumped mode is high (and thus the fluctuations small), most of the damping originates from fluctuations in the unpumped mode. Tunneling is slightly enhanced compared to the standing-wave lattice, which is consistent with the shape of the effective potential: A broader potential results in slightly larger hopping matrix elements. However, stronger damping can be observed whenever tunneling gets enhanced as the coupling to the unpumped mode increases. Ensemble averages over 100 Monte Carlo wave-function trajectories. Parameters: $U_0=-\omega_R$, $\alpha_c=\sqrt{12}$, $\Delta_c=U_0-\kappa$, and $\kappa=600\omega_R$ (upper plot) and $\kappa=200\omega_R$ (lower plot), respectively.

the field operators appearing in (31) using a suitable set of localized Wannier functions which can be obtained from Bloch eigenfunctions of the single-particle Hamiltonian [47]. In the limit of particle energies well below the trap frequency $\omega_T=\sqrt{4V_0E_R}/\hbar$ (V_0 is the potential depth), the expansion may be even restricted to the lowest Bloch band [1,2]. In many cases, this approximation is very good and thus the consideration of higher bands is not necessary—even in the presence of any direct particle-particle interaction. Although one has to take extra care in choosing the correct Wannier basis, to some extent this procedure can still be applied when the optical lattice is generated not by a classically described coherent light field but rather by a quantized standing-wave mode of an optical resonator [14–16,50]. As long as the photon-number uncertainty is much less than the average photon number, a self-consistent average potential depth can be chosen to calculate suitable particle basis states for the expansion of the field operator. The relevant parameters like tunneling and

on-site energies then only weakly depend on the photon-number fluctuations in the mode. Note that this procedure gets doubtful or even inapplicable if the cavity damping rate gets comparable with the time scale of particle motion or when only few photons are present in the field mode generating the potential.

Naturally, one is tempted to try an analogous approach for the ring-cavity lattice formed by two quantized light modes as a first step. In the case of symmetric pump, only the cosine mode is excited in the empty cavity, and thus we can start with a Wannier basis involving only the lowest band of the highly excited cosine-mode potential. Interestingly, we find that within this ansatz a restriction of the particle dynamics to the lowest band immediately implies a complete decoupling of the sine mode from the dynamics. The ring resonator then behaves exactly as a standing-wave cavity because the possibility of a lattice displacement is neglected by this ansatz. In principle, one needs to consider displaced Wannier functions, which is not an obvious task: Treating the displacement δx as a self-consistent c-number (in the spirit of the afore discussed self-consistent potential depth) would result in a vanishing displacement for all times, if it was zero initially. This obviously does not reproduce the scattering of photons into the unpumped mode. On the other hand, differently displaced Wannier functions—which would take into account that the Hamiltonian modifies the lattice—are not orthogonal and hence do not form a suitable basis for a lattice model. One way to overcome this problem by taking into account higher Bloch bands will be presented in Sec. IV B, where we show that the corresponding cooperative tunneling and scattering processes are needed for a correct physical modeling of the dynamics.

A. Single-band model

As just discussed, in a first attempt we restrict the particle dynamics in the Hamiltonian (31) to the lowest Bloch band in the potential generated solely by the strongly pumped cosine mode. The field operator is thus approximated by

$$\Psi(x) \simeq \sum_i w_0(x - x_i) b_i, \tag{33}$$

where the bosonic operators $b_i^{(\dagger)}$ destroy (create) a particle at the ith lattice site and $w_0(x - x_i) =: w_i^0(x)$ denotes the zeroth-band Wannier function localized there. The expanded Hamilton operator (31) then reads

$$\begin{aligned} H = &\sum_{i,j} E_{ij} b_i^\dagger b_j + \hbar U_0 (a_c^\dagger a_c - a_s^\dagger a_s) \sum_{i,j} J_{ij} b_i^\dagger b_j \\ &+ \hbar U_0 N a_s^\dagger a_s + \frac{\hbar U_0}{2} (a_c^\dagger a_s + a_c a_s^\dagger) \sum_{i,j} \tilde{J}_{ij} b_i^\dagger b_j \\ &- \hbar \Delta_c (a_c^\dagger a_c + a_s^\dagger a_s) - i\hbar \eta_c (a_c - a_c^\dagger), \end{aligned} \tag{34}$$

where we have defined the matrix elements

$$E_{ij} := \left\langle w_i^0, \frac{p^2}{2m} w_j^0 \right\rangle, \tag{35a}$$

$$J_{ij} := \langle w_i^0, \cos^2(kx) w_j^0 \rangle, \tag{35b}$$

$$\tilde{J}_{ij} := \langle w_i^0, \sin(2kx) w_j^0 \rangle. \tag{35c}$$

As the next-nearest-neighbor matrix elements are at least one order of magnitude smaller than their nearest-neighbor counterparts, we keep only the latter. Looking closely at the above expressions, the most interesting point to note is that $\tilde{J}_{ik} = 0 \ \forall i,k$ due to symmetry. This can easily be seen analytically: The product $w_0(x - x_i) w_0(x - x_j)$ is symmetric about the point $(x_i + x_j)/2$ and has compact support due to the exponential localization of the Wannier functions. The function $\sin(2kx)$, on the other hand, is an odd function with respect to the extrema of the potential. The integrand appearing when evaluating the scalar product (35c) is thus an odd function and therefore the integral over $\mathbb{R}$ vanishes. Hence the Bose-Hubbard-type Hamiltonian reads

$$\begin{aligned} H = &E_0 N + E B + [\hbar U_0 (a_c^\dagger a_c - a_s^\dagger a_s)](J_0 N + J B) \\ &+ \hbar U_0 N a_s^\dagger a_s - \hbar \Delta_c (a_c^\dagger a_c + a_s^\dagger a_s) - i\hbar \eta_c (a_c - a_c^\dagger), \end{aligned} \tag{36}$$

where we have defined the particle number operator N and the hopping operator $B := \sum_i (b_i^\dagger b_{i+1} + b_{i+1}^\dagger b_i)$. E_0, J_0 (E, J) denote the on-site (nearest-neighbor off-site) matrix elements (35).

Note the lack of terms accounting for scattering into the sine mode in this Hamiltonian. The unpumped mode thus completely decouples from the system dynamics and simply decays to its vacuum state. Hence there will be no difference to the standing-wave cavity case after this decay. Mathematically, this can be seen by explicitly writing the Heisenberg equations for the sine mode,

$$\dot{a}_s = (i\{\Delta_c + U_0[(J_0 - 1)N + J B]\} - \kappa) a_s, \tag{37a}$$

$$\dot{a_s^\dagger a_s} = -2\kappa a_s^\dagger a_s. \tag{37b}$$

In the bad-cavity limit, when the field relaxes almost instantaneously to its steady-state value, both quantities vanish. To capture more of the physics of the ring resonator, higher bands need to be included. This will be done in Sec. IV B.

As the single-mode model has been extensively treated in previous literature, we will not discuss this much further. But is this result a bug or a feature? Mathematically, the decoupling of the sine mode originates from the even symmetry of the lowest-band Wannier functions, which we used as our basis. Physically, one could argue that tunneling between sites within a band does not invoke any force or momentum transfer and thus introduces no coupling or scattering to the empty sine mode. Hence the model can be at least self-consistent for a superfluid phase strictly limited to a single band. Of course, adding on-site interactions already destroys this argument as these are connected to changes of the local wave functions which amounts to the appearance of higher-band contributions. These will couple to the sine mode as seen in the numerical examples in Sec. II and the appearance of sine photons thus would herald the breakdown of zeroth-band superfluidity.

B. Multiband model

In order to incorporate excitations of the unpumped mode we have to allow for tunneling events from one site to a neighboring site with a simultaneous generation of a photon in the sine mode. This means that the final-particle wave function

is shifted with respect to the unperturbed basis: As the Wannier states corresponding to the cosine potential form an orthogonal basis set, mathematically this amounts, of course, to the admixture of higher-band Bloch functions in the dynamics. One might at this point be tempted to state that the zeroth-band motion will thus largely decouple from the unpumped sine mode whenever the excitation energy to the next band is sufficiently large. However, one has to be more careful here. Actually, the lowest-band approximation in the cosine potential does not necessarily coincide with the lowest-band approximation for the ring cavity. During the time evolution the potential can get shifted relative to the unperturbed potential generated by the pump field. Hence, despite possessing contributions from higher-band wave functions, the particle can still have an energy corresponding to the lowest band as its wave function is simply a shifted lowest-band Wannier state.

Mathematically, one can estimate such contributions by expanding the lowest-band Wannier functions of a shifted lattice in the Wannier functions (including higher bands) of the original one, which, as said, form a complete basis set. We see, that to lowest order only the first antisymmetric band significantly contributes. This can be easily checked. If $w_0(x - x_i)$ is the lowest-band Wannier function localized at the ith lattice site of the unperturbed lattice, the Taylor expansion of a slightly shifted Wannier function to lowest order in the shift δx reads

$$w_0(x - x_i - \delta x) \simeq w_0(x - x_i) - \delta x w_0'(x - x_i). \quad (38)$$

The first derivative of the ground-state Wannier function is antisymmetric and thus the first band gets involved.

Let us therefore develop an improved version of the previously derived Bose-Hubbard model, which includes the important additional physics originating from the ring-cavity geometry. To this end, we reconsider the original Hamiltonian (3) and assume a sufficiently strong coherent field α_c in the cosine mode so that its quantum properties can be ignored and only the sine mode needs a description by an operator a. The Hamiltonian thus reads

$$H = \frac{p^2}{2m} + \hbar U_0(|\alpha_c|^2 - a^\dagger a)\cos^2(kx) - \hbar(\Delta_c - U_0)a^\dagger a + \frac{\hbar U_0}{2}\sin(2kx)(\alpha_c^* a + \alpha_c a^\dagger). \quad (39)$$

For very low photon numbers in the sine mode, we can neglect its contribution proportional to $a^\dagger a$ to the potential depth and get:

$$V(x) = \hbar U_0(|\alpha_c|^2 - a^\dagger a)\cos^2(kx) \simeq \hbar U_0|\alpha_c|^2\cos^2(kx). \quad (40)$$

This Hamiltonian is closely related to an optomechanical coupling as used in Ref. [17], but here we have a periodic trapping potential for the particle motion. During the dynamics, the classical periodic potential is modified through the scattering term. A photon in the sine mode essentially leads to a broadening of the effective potential, which lowers the ground-state energy and modifies the tunnel coupling to neighboring sites.

From a physics point of view, the dynamics induced by this Hamiltonian in several aspects resembles the case of particle motion in a standing-wave light field across a high-finesse resonator [31,48], where a self-organization of the particles in two possible patterns filling every second lattice site can occur. Position-dependent light scattering modifies the optical potential so the occupied sites deepen. The difference to our system is the symmetry of the scattering term, which here is antisymmetric with respect to the extrema of the classical potential. So instead of resulting in a state-dependent deepening of the lattice, the scattered light shifts the position of the lattice sites with respect to the classical potential. In a Bloch expansion with respect to the classical potential this shift amounts to contributions of higher bands like any interaction term would do.

To obtain a lattice model we expand the field operator to

$$\Psi(x) = \sum_i \sum_n b_i^n w_i^n(x), \quad (41)$$

where b_i^n destroys a particle in the nth band at the ith well and w_i^n denotes the corresponding Wannier function. Neglecting any direct particle-particle interaction, we obtain the second-quantized version of the Hamiltonian (39),

$$H = \sum_{n,m}\sum_{i,j} E_{ij}^{nm} b_i^{n\dagger} b_j^m - \hbar(\Delta_c - \hat{N}U_0)a^\dagger a + \frac{\hbar U_0}{2}\sum_{n<m}\left(\tilde{J}^{nm}\tilde{T}^{nm} + \sum_{i\neq j}\tilde{J}_{ij}'^{nm}\tilde{B}_{ij}^{nm}\right)(\alpha_c^* a + \alpha_c a^\dagger), \quad (42)$$

where we have defined the operators

$$\hat{N} := \sum_n \sum_i b_i^{n\dagger} b_i^n \equiv Nid, \quad (43a)$$

$$\tilde{T}^{nm} := \sum_i \left(b_i^{n\dagger} b_i^m + b_i^{m\dagger} b_i^n\right), \quad (43b)$$

$$\tilde{B}_{ij}^{nm} := b_i^{n\dagger} b_j^m + b_j^{m\dagger} b_i^n. \quad (43c)$$

$\hat{N}$ is the number operator and proportional to the identity operator id as the total number of particles is conserved. $\tilde{T}^{nm}$ describes transitions between two bands within one well, whereas $\tilde{B}_{ij}^{nm}$ accounts for hopping between two wells together with a change of the band. The corresponding matrix elements read

$$E_{ij}^{nm} := \left\langle w_i^n, \left(\frac{p^2}{2m} + \hbar U_0|\alpha_c|^2\cos^2(kx)\right) w_j^m \right\rangle, \quad (44a)$$

$$\tilde{J}^{nm} := \langle w_i^n, \sin(2kx) w_i^m \rangle, \quad (44b)$$

$$\tilde{J}_{ij}'^{nm} := \langle w_i^n, \sin(2kx) w_j^m \rangle. \quad (44c)$$

Note that in-well transitions between bands without photon exchange are prohibited as $E_{ii}^{nm} = 0\ \forall\, n \neq m$.

C. Two-band lattice model

The Hamiltonian (42) is still complex and hard to solve completely. Hence, we will first try to highlight the basic physics of particle motion and lattice shifts in an as-simple-as-necessary model and restrict the particle motion to two bands. As pointed out earlier, to lowest order the first excited band gets coupled. It will be the superpositions of odd- and even-parity eigenstates within one well which scatter a coherent field into

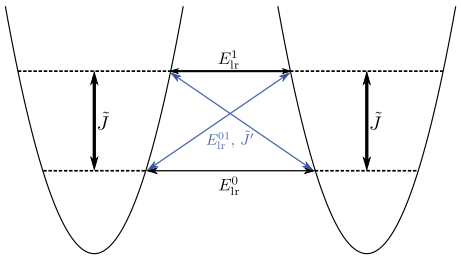

FIG. 7. (Color online) Schematic view of some processes appearing in the Hamiltonian (45) for two chosen lattice sites. The width of the arrows corresponds to the amplitude of the process, i.e., the magnitude of the matrix elements (44).

the sine mode with nonvanishing amplitude $\langle a \rangle$. Keeping only the on-site and nearest-neighbor matrix elements and defining $E^n := E^{nn}_{ii}$, $\tilde{J} := \tilde{J}^{01}$ and $\tilde{J}' := \tilde{J}'^{01}_{i,i+1}$ the Hamiltonian reads

$$H = \sum_{\substack{n=0,1\\ i}} E^n b_i^{n\dagger} b_i^n + \sum_{\substack{n,m=0,1\\ \langle i,j\rangle}} E^{nm}_{i,j} b_i^{n\dagger} b_j^m + \frac{\hbar U_0}{2}\left(\tilde{J}\tilde{T} + \sum_{\langle i,j\rangle} \tilde{J}'\tilde{B}_{ij}\right)(\alpha_c^* a + \alpha_c a^\dagger) - \hbar(\Delta_c - \hat{N}U_0) a^\dagger a. \tag{45}$$

$\tilde{T} := \tilde{T}^{01}$ and $\tilde{B} := \tilde{B}^{01}_{i,i+1}$ describe on-site (off-site) parity changes.

Here we make a short remark concerning very deep potentials. There the hierarchy

$$|\tilde{J}| \gg |E^1| \gg |E^0| \sim |\tilde{J}'| \gg \left|E^{01}_{i,i+1}\right| \tag{46}$$

holds. Hence, tunneling happens preferably via excitation to the first band and subsequent tunneling within this band (see also Figs. 7 and 8). However, one has to be conscious that a too-large effective coupling strength invalidates the two-band model as even higher bands need to be taken into account. See Fig. 9 for a situation where the two-band model fails, whereas the three-band version allows for reproducing the results of the full Monte Carlo simulations (cf. Sec. V).

Most of the new physics involving tunneling with light scattering and hopping between bands can be already seen in a truncated two-site version of the model. Labeling the two sites by indices l and r for left and right, the Heisenberg equation of motion for the field then explicitly reads (neglecting the input noise operator)

$$\dot{a} = [i(\Delta_c - NU_0) - \kappa]a - i\frac{\alpha_c U_0}{2}(\tilde{J}\tilde{T} + \tilde{J}'\tilde{B}) \tag{47}$$

and its steady-state solution

$$a_{ss} = \frac{-i\frac{\alpha_c U_0}{2}(\tilde{J}\tilde{T} + \tilde{J}'\tilde{B})}{\kappa - i(\Delta_c - NU_0)}. \tag{48a}$$

For the photon number one obtains

$$(a^\dagger a)_{ss} = \frac{\frac{|\alpha_c|^2 U_0^2}{4}(\tilde{J}\tilde{T} + \tilde{J}'\tilde{B})^2}{\kappa^2 + (\Delta_c - NU_0)^2} \simeq \frac{|\alpha_c|^2}{4}\frac{U_0^2}{\Delta_c^2 + \kappa^2}(\tilde{J}\tilde{T} + \tilde{J}'\tilde{B})^2, \tag{48b}$$

where the latter is valid for $|U_0| \ll |\Delta_c|$.

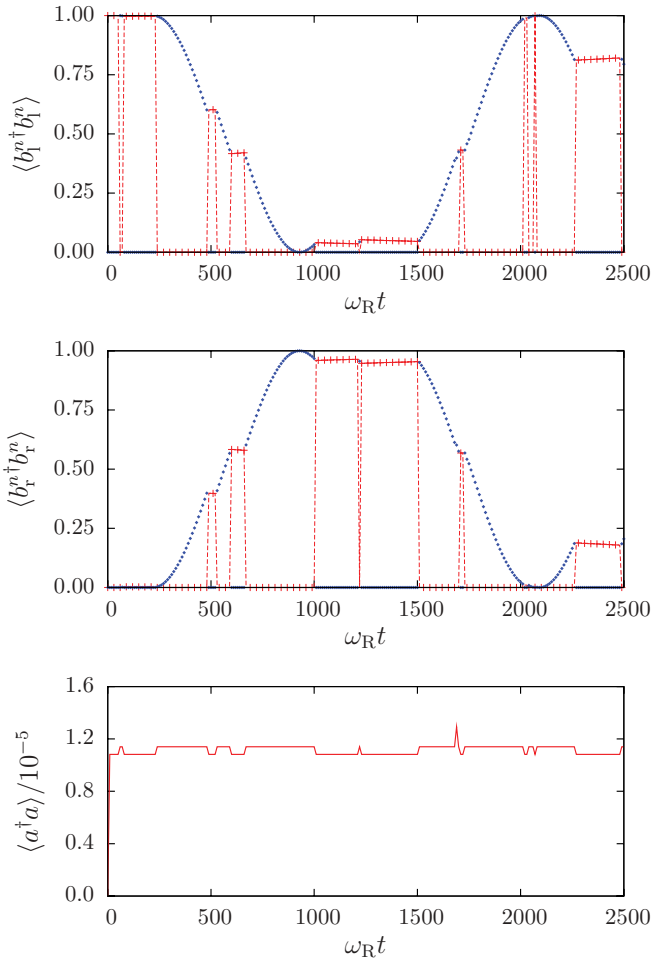

FIG. 8. (Color online) Single Monte Carlo trajectory of the two-band Bose-Hubbard model for a very deep potential ($V_0 = 50E_R$) and two wells. [Red crosses (blue dots)] Expectation value of the particle number in the zeroth (first) band within each well. As zeroth-band tunneling is neglectable on the simulated time scale, the population within this band does not change considerably (horizontal lines). Only the first-band tunneling has a significant effect and subsequently modifies the zeroth-band distribution within the two lattice sites. Parameters: $U_0 = -2\omega_R$, $\kappa = 500\omega_R$, $\alpha_c = 5$, and $\Delta_c = U_0 - \kappa$.

For large resonator damping constants κ, where the particle dynamics follows the field adiabatically, the localized states within one band radiate a field with zero amplitude,

$$\left\langle w_i^n \middle| a_{ss} \middle| w_i^n \right\rangle = 0 \; \forall \, i,n \tag{49}$$

but nonvanishing photon number. Indeed, for one particle, the photon number is the same for all four localized basis states,

$$\langle\psi|(\tilde{J}\tilde{T} + \tilde{J}'\tilde{B})^2|\psi\rangle = \tilde{J}^2 + \tilde{J}'^2 \quad \forall\, |\psi\rangle \in \left\{ \left| w_i^n \right\rangle | i \in \{\mathrm{l,r}\}, n \in \{0,1\} \right\}. \tag{50}$$

As pointed out before, the ground state will always have a non-negligible contribution of the first band. Therefore it is convenient to switch to the basis of even and odd localized states,

$$|\psi^{\pm}_{\mathrm{l,r}}\rangle := \frac{1}{\sqrt{2}}\left(\left|w^0_{\mathrm{l,r}}\right\rangle \pm \left|w^1_{\mathrm{l,r}}\right\rangle\right) \tag{51}$$

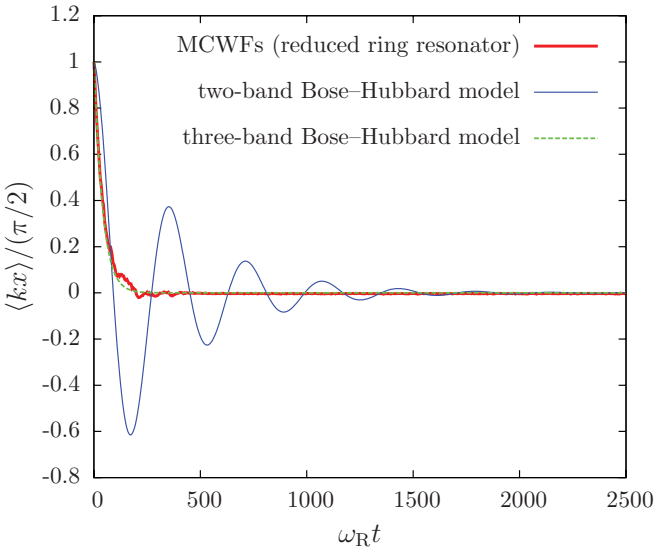

FIG. 9. (Color online) Average position of the particle computed with Monte Carlo simulations (ensemble average over 150 trajectories) of the reduced model (ii) presented in Sec. V and with the two- and three-band lattice models. The two-band version fails, whereas the inclusion of the next band reproduces the correct behavior. Parameters: $U_0 = -2\omega_R$, $\alpha_c = \sqrt{12.5}$, $\Delta_c = U_0 - \kappa$, and $\kappa = 10\omega_R$.

which radiate an approximately coherent field $|\pm\alpha\rangle$ with amplitude

$$\alpha = \frac{-i\frac{\alpha_c U_0}{2}\tilde{J}}{\kappa - i(\Delta_c - NU_0)} \tag{52}$$

into the resonator. Strictly speaking, this is valid only as long $\tilde{J}^2 \gg \tilde{J}'^2$. However, this does not bring about any further restriction on the potential depth $V_0 = \hbar|U_0||\alpha_c|^2$ since already for $V_0 = 5E_R$ (for shallower potentials, the localized Wannier states cannot be properly defined [2]) the squared matrix elements already differ by three orders of magnitude, $\tilde{J}'^2/\tilde{J}^2 \sim 0.002$. This difference gets much more pronounced for deeper and deeper lattices. We can thus safely assume $\tilde{J}^2 + \tilde{J}'^2 \simeq \tilde{J}^2$.

The basis decomposition of an arbitrary particle state in one well reads

$$\sqrt{1-|\varepsilon|^2}|w_i^0\rangle + \varepsilon|w_i^1\rangle = \frac{\sqrt{1-|\varepsilon|^2}+\varepsilon}{\sqrt{2}}|\psi_i^+\rangle + \frac{\sqrt{1-|\varepsilon|^2}-\varepsilon}{\sqrt{2}}|\psi_i^-\rangle. \tag{53}$$

The vanishing field amplitude for a particle in a parity eigenstate [$|\varepsilon| \in (0,1)$] can thus be explained as a consequence of destructive interference: The two components of the particle state radiate a field $|\alpha\rangle$ and a field $|-\alpha\rangle$, respectively. The resulting field state described by the reduced density matrix $\rho \propto |\alpha\rangle\langle\alpha| + |-\alpha\rangle\langle-\alpha|$ has a vanishing amplitude expectation value but a nonvanishing photon-number expectation value, cf. the broadened adiabatic potential derived in Sec. III which can be explained as an average effect of the two shifts.

The jump operator $\sqrt{2\kappa}a$ can act as a parity-switch operator: Suppose the particle being in the lowest band of the left well prior to the jump,

$$|\psi\rangle \propto |\psi_l^+\rangle|\alpha\rangle + |\psi_l^-\rangle|-\alpha\rangle. \tag{54a}$$

Directly after the jump, the system state reads

$$a|\psi\rangle \propto |\psi_l^+\rangle|\alpha\rangle - |\psi_l^-\rangle|-\alpha\rangle, \tag{54b}$$

which corresponds to the antisymmetric particle state ($\varepsilon = 1$ above). Figures 8, 10, and 11 show single Monte Carlo trajectories depicting this behavior. More generally, quantum jumps result in a loss of the coherences in the system state [48]: During the coherent evolution the composed system state reads

$$|\psi_t\rangle = c_l^+(t)|\psi_l^+\rangle|\alpha\rangle + c_l^-(t)|\psi_l^-\rangle|-\alpha\rangle + c_r^+(t)|\psi_r^+\rangle|\alpha\rangle + c_r^-(t)|\psi_r^-\rangle|-\alpha\rangle. \tag{55a}$$

Acting with the jump operator $\propto a$ on this state causes two phase shifts destroying the coherences:

$$a|\psi_t\rangle \propto c_l^+(t)|\psi_l^+\rangle|\alpha\rangle - c_l^-(t)|\psi_l^-\rangle|-\alpha\rangle + c_r^+(t)|\psi_r^+\rangle|\alpha\rangle - c_r^-(t)|\psi_r^-\rangle|-\alpha\rangle. \tag{55b}$$

For the ensemble average over many quantum trajectories this effects leads to dephasing and thus to a damping of the tunneling oscillations.

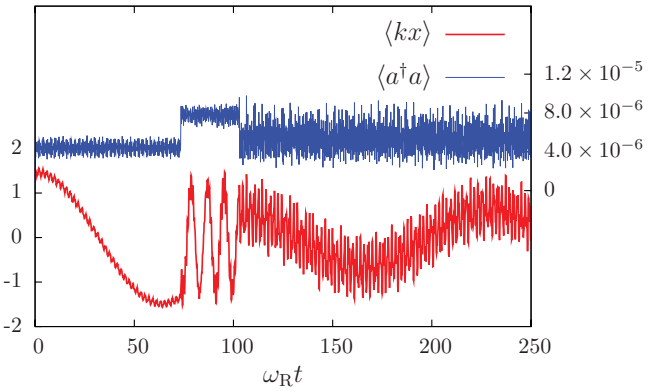

FIG. 10. (Color online) Sample trajectory of the reduced model (ii) presented in Sec. V showing the position expectation value $\langle kx\rangle$ (left y axis, lower curve) and $\langle a^\dagger a\rangle$ (right y axis, upper curve). The two quantum jumps occurring at $\omega_R t \sim 70$ and $\omega_R t \sim 100$ are clearly visible: The photon number in the mode and the occupied band of the particle are changed simultaneously as seen from the sudden change of the oscillation frequency and amplitude between the potential wells. Here even higher bands are excited. After the fast oscillation between the wells the particle gets trapped again, but in a higher excited state, as can be seen from the higher amplitude. Furthermore, the photon-number variance is much more pronounced. Parameters: $U_0 = -2\omega_R$, $\alpha_c = \sqrt{6}$, $\Delta_c = U_0 - \kappa$, and $\kappa = 500\omega_R$.

V. COMPARISON WITH FULL MONTE CARLO WAVE-FUNCTION SIMULATIONS

So far our treatment relied on a series of analytic approximations which allowed us to predict a wealth of new physical phenomena. To get a first check on the validity and the prediction power of these models we compare them to "full" numerical simulations of the single-particle dynamics in a ring resonator. They are carried out in a momentum- and photon-number basis truncated at sufficiently high numbers to include all the relevant physics. In addition to a quantitative

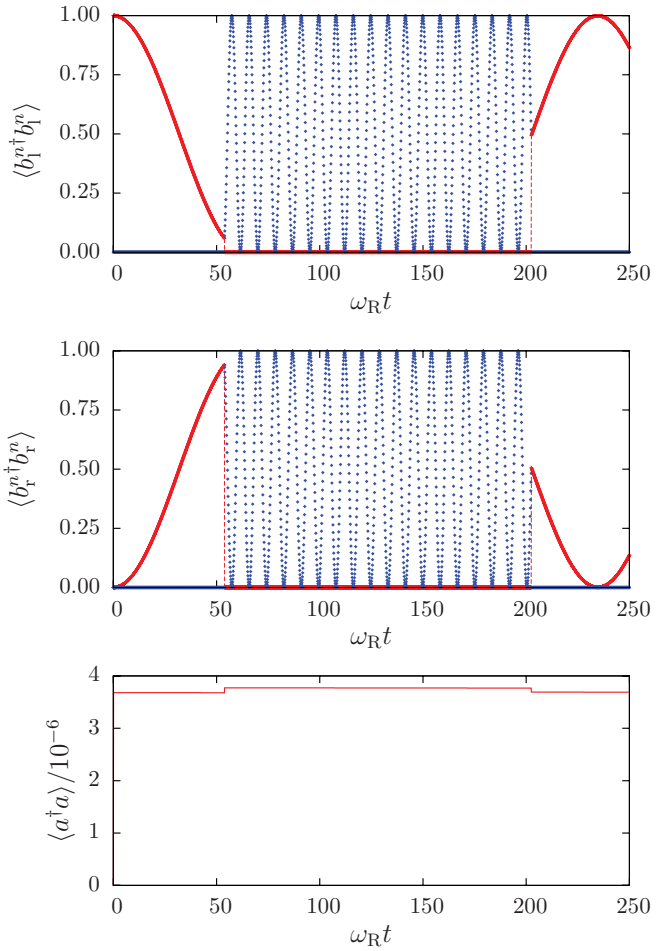

FIG. 11. (Color online) Single Monte Carlo trajectory of the two-band Bose-Hubbard model for a shallow potential ($V_0 = 12E_R$) and two wells. [Red solid line (blue dots)] Expectation value of the particle number in the zeroth (first) band within each well. Quantum jumps in the photon number can indeed trigger parity changes of the particle as sketched in the text [Eqs. (54)]. The different tunneling time scales for the two bands can be seen. This trajectory can be regarded as a Bose-Hubbard equivalent to Fig. 10; the parameters are the same as described in the caption.

check for the analytic approximations these simulations also give nice qualitative insights into the microscopic origins of the observed phenomena. These simulations with at least three independent quantum degrees of freedom are generally very expensive in computer memory and time. They were performed using a Monte Carlo wave-function simulation algorithm as implemented in the locally developed C++QED framework [51],[1] which is highly optimized for efficient memory handling and time-evolution speed. For technical reasons we swapped the role of the the two modes in the simulations, the sine mode is thus pumped, and therefore the two potential wells (periodic boundary conditions) are located at $kx = \pm\pi/2$.

We performed Monte Carlo simulations of three different systems:

(i) the full ring resonator as described by the Hamilton operator (3),

(ii) the reduced system with the pumped mode set to a coherent state described by the Hamiltonian (39) [without the approximation (40)], and, for comparison,

(iii) the pumped standing-wave resonator.

Additionally, we performed as well a series of Monte Carlo simulations of

(iv) the Bose-Hubbard model (45) to demonstrate the effects of quantum jumps on the particle parity. However, for the time evolution of the density matrix this much lower-dimensional model was alternatively solved by directly integrating the full master equation.

In order to reobtain the (approximately) same potential depth in the full system (i) we set $\eta_c = |\alpha_c|\sqrt{\kappa^2 + (\Delta_c - U_0)^2}$. In all simulations, the particle was initially in a Gaussian state (momentum-space simulations) or in the lowest Wannier state (lattice model), respectively, localized in the right well. Note that due to the periodic boundary conditions, tunneling is enhanced by a factor of 2 in all numerical simulations. For comparison, we have taken this into account in the Bose-Hubbard model as well and have doubled all hopping matrix elements.

In Fig. 12 the standing-wave lattice is compared to the ring resonator. Although the unpumped mode is hardly populated—$\langle a^\dagger a \rangle \sim 1.4 \times 10^{-5}$—its impact on the particle is well pronounced. We see a significantly faster decay of coherent tunneling due to the presence of the second mode as source of decoherence. One might also recognize a slightly faster tunneling time due to the modified effective potential but this would require a much larger ensemble to be quantitatively checked. Here the validity condition for the approximation (40) is very well fulfilled. Note that for the

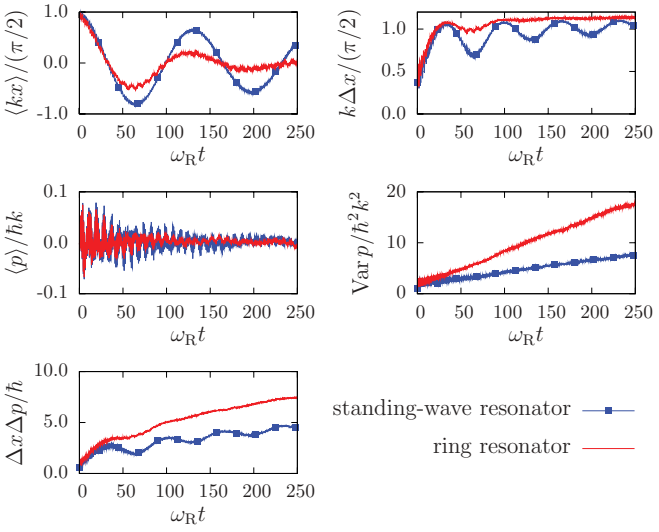

FIG. 12. (Color online) Comparison of the standing-wave resonator [model (iii)] and the ring resonator [model (i)] for one particle. Ensemble average over 250 trajectories. Parameters: $U_0 = -3\omega_R$, $\alpha_c = 2$, $\Delta_c = U_0 - \kappa$, and $\kappa = 400\omega_R$.

[1]The latest—and strongly improved with respect to the previous one described in Ref. [51]—release of the framework (version 2) can be downloaded from the project's homepage www.uibk.ac.at/th-physik/qo/research/cppqed.html or directly at www.cppqed.sourceforge.net.

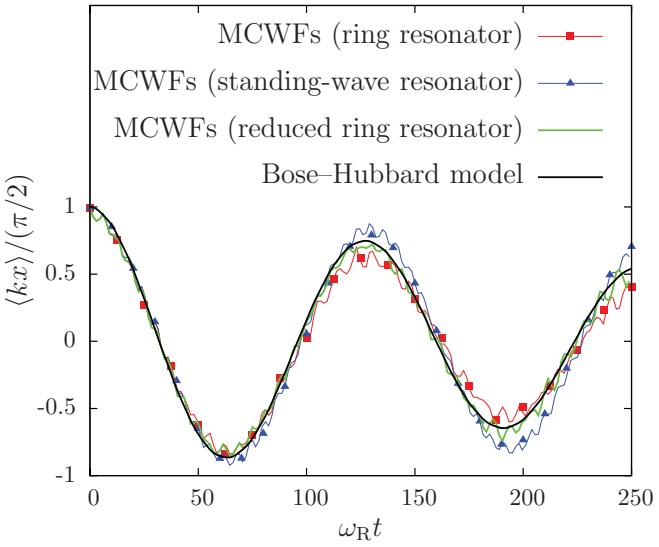

FIG. 13. (Color online) Average position of the particle computed with the four models described in Sec. V. For the Bose-Hubbard model the population imbalance $\langle N_r\rangle - \langle N_l\rangle$ has been plotted. Ensemble average over 100 trajectories. Parameters: $U_0 = -\omega_R$, $\alpha_c = \sqrt{12}$, $\Delta_c = U_0 - \kappa$, and $\kappa = 400\omega_R$.

parameters used in the figure the average photon number in the pumped mode generating the optical potential was only 4, which, however, still proves enough for the classical (coherent state) approximation for this mode amplitude to give qualitatively similar results. As particle motion is based essentially on tunneling in the low temperature limit, scattering to the unpumped mode can be viewed as an effective friction mechanism in the model.

Figure 13 shows the particle hopping between two sites computed from all four aforementioned models. The reduced system (ii) is indeed a good approximation for sufficiently large $|\alpha_c|$. Since the effective coupling is not too large the two-band Bose-Hubbard model can remarkably well reproduce the results. However, as the coupling increases the two-band approximation turns out to be too restrictive. Including higher bands in such cases becomes absolutely necessary. Such a situation is depicted in Fig. 9, where taking into account the second excited band allows for reproducing the predictions of model (ii).

Looking at the microscopic origin of the dephasing and decoherence, the crucial effect of quantum jumps on these can be seen in Figs. 8, 10, and 11. The parity swaps predicted in Eqs. (54) can be nicely seen and the different tunneling time scales corresponding to the two bands are clearly visible. As the jump times have a strong random contribution, the source of dephasing thus gets very obvious. Actually, a related mechanism might also occur in free-space optical lattices if collisions invoke higher bands in the particle dynamics. Note that transitions between the bands visible in changes of the tunnel oscillation frequency are also accompanied by jumps in the photon number, which provides for real-time monitoring of the band populations.

Finally, we demonstrate that the Bose-Hubbard model can capture a great deal of the underlying physics if several bands are included. This is depicted in Fig. 14 which exhibits a

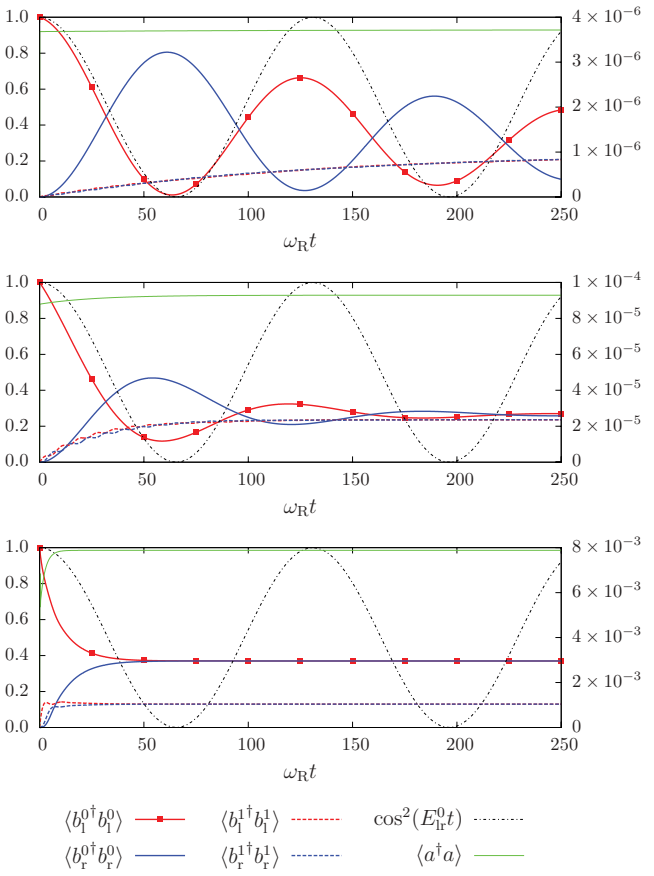

FIG. 14. (Color online) Population evolution from the Bose-Hubbard-like lattice model for a fixed potential depth $V_0 = 12E_R$. The different time scales for the two bands are clearly visible. The particle was initially in the lowest band and located in the left well. The black dash-dotted line shows the tunneling Rabi oscillation for the lowest band without any coupling to the mode, i.e., $H = E_{lr}^0 b_l^{0\dagger} b_r^0 + \text{H.c.}$, for comparison. (Left y axis) Populations; (right y axis) photon number. As the parameters are similar to the ones used in Fig. 6, these plots give a microscopic band interpretation of the particle motion presented there. Parameters: $U_0 = -2\omega_R$, $\alpha_c = \sqrt{6}$, $\Delta_c = U_0 - \kappa$, and $\kappa = (500, 100, 10)\omega_R$ from top to bottom.

significant excitation of the first excited band in steady state. This is consistent with the full simulations above, where a similar heating to higher bands can be observed, cf. Fig. 12.

VI. CONCLUSIONS

We have developed several approximative analytical models to describe the dynamics of a quantum particle in an optical lattice which is generated by counterpropagating fields in a high-Q ring resonator. A standard single-band description in terms of Bloch or Wannier functions calculated from the unperturbed optical potential predicts frictionless tunneling motion of the particles and long-range coherence of the corresponding wave function. However, this approximation misses most of the essential physics. Already a perturbative inclusion of the first excited band reveals particle hopping between bands and sites accompanied by photon scattering into empty field modes as a key mechanism to provide for a realistic description of the dynamics. Even for very

small photon scattering rates it leads to dephasing of tunnel oscillations and decoherence of the wave function. This will strongly diminish coherent transport together with heating of particle motion. In the perturbative approach it essentially leads to a modified effective potential shape and a phase-decay term. Note that this term, although being much smaller in a free-space-lattice setup, will finally also pose limits on obtainable coherence lengths and acceleration sensitivity in large free-space optical lattices. Microscopically, dephasing can be traced back to the strongly band (energy) dependent tunneling times, so even very small contributions of different bands lead to significant time shifts of tunnel oscillations. The corresponding approximative models which we developed will give a basis for future many-body generalizations of the model involving short- and long-range interactions between different particles. The interactions mediated by the scattered photons play a very similar role as phonons in real solid-state systems and thus can be a useful handle to shape and study long-range interactions in cold-atom optical lattices. As the photons scattered by different particles into the same mode even at long distances will interfere, they can lead to nonlocal momentum-space pairing of particle motion. The interaction will also help to establish long-range order, which will be particularly the case for the transverse-pump case, where no *a priori* order is prescribed by the field modes and the atoms can self-arrange in a supersolid with diagonal and off-diagonal order.

In addition to modifying the dynamics and steady state of the particles, the scattering modes also provide for a basis for a real-time monitoring system of the particles to study the transition between different quantum phases or quantum models of transport in lattices with destruction of the system. This would require including direct local interactions in addition, which should be possible at least in the few-band limit of the model. As we centrally only need polarizable point particles, corresponding effects could as well be observed with molecules or even nanoparticles which are optically trapable.

ACKNOWLEDGMENTS

This work has been supported by the Austrian Science Fund FWF through projects P20391 and F4013. We thank Tobias Grießer, Matthias Sonnleitner, and Hashem Zoubi for helpful discussions.

[1] D. Jaksch, C. Bruder, J. I. Cirac, C. W. Gardiner, and P. Zoller, Phys. Rev. Lett. **81**, 3108 (1998).
[2] D. Jaksch and P. Zoller, Ann. Phys. **315**, 52 (2005).
[3] I. Bloch, J. Dalibard, and W. Zwerger, Rev. Mod. Phys. **80**, 885 (2008).
[4] M. Lewenstein, L. Santos, M. A. Baranov, and H. Fehrmann, Phys. Rev. Lett. **92**, 050401 (2004).
[5] J. K. Asboth, H. Ritsch, and P. Domokos, Phys. Rev. Lett. **98**, 203008 (2007).
[6] P. Domokos and H. Ritsch, J. Opt. Soc. Am. B **20**, 1098 (2003).
[7] P. Horak and H. Ritsch, Phys. Rev. A **63**, 023603 (2001).
[8] T. Bourdel, T. Donner, S. Ritter, A. Öttl, M. Köhl, and T. Esslinger, Phys. Rev. A **73**, 043602 (2006).
[9] Y. Colombe, T. Steinmetz, G. Dubois, F. Linke, D. Hunger, and J. Reichel, Nature (London) **450**, 272 (2007).
[10] S. Gupta, K. L. Moore, K. W. Murch, and D. M. Stamper-Kurn, Phys. Rev. Lett. **99**, 213601 (2007).
[11] K. Baumann, C. Guerlin, F. Brennecke, and T. Esslinger, Nature **464**, 1301 (2010).
[12] D. Nagy, G. Kónya, G. Szirmai, and P. Domokos, Phys. Rev. Lett. **104**, 130401 (2010).
[13] D. Meiser, J. Ye, and M. J. Holland, New J. Phys. **10**, 073014 (2008).
[14] C. Maschler and H. Ritsch, Phys. Rev. Lett. **95**, 260401 (2005).
[15] C. Maschler, I. B. Mekhov, and H. Ritsch, Eur. Phys. J. D **46**, 545 (2008).
[16] J. Larson, S. Fernández-Vidal, G. Morigi, and M. Lewenstein, New J. Phys. **10**, 045002 (2008).
[17] R. J. Schulze, C. Genes, and H. Ritsch, Phys. Rev. A **81**, 063820 (2010).
[18] C. Maes, J. K. Asbóth, and H. Ritsch, Opt. Express **15**, 6019 (2007).
[19] J. Klinner, M. Lindholdt, B. Nagorny, and A. Hemmerich, Phys. Rev. Lett. **96**, 023002 (2006).
[20] S. Slama, S. Bux, G. Krenz, C. Zimmermann, and P. W. Courteille, Phys. Rev. Lett. **98**, 053603 (2007).
[21] G. Hechenblaikner, M. Gangl, P. Horak, and H. Ritsch, Phys. Rev. A **58**, 3030 (1998).
[22] M. Gangl and H. Ritsch, Phys. Rev. A **61**, 043405 (2000).
[23] D. Kruse, M. Ruder, J. Benhelm, C. von Cube, C. Zimmermann, P. W. Courteille, T. Elsässer, B. Nagorny, and A. Hemmerich, Phys. Rev. A **67**, 051802(R) (2003).
[24] D. Meiser, J. Ye, and M. Holland, in *APS Meeting Abstracts* (2009), p. 1121.
[25] R. Bonifacio, Opt. Commun. **146**, 236 (1998).
[26] T. Grießer, H. Ritsch, M. Hemmerling, and G. R. M. Robb, Eur. Phys. J. D **58**, 349 (2010).
[27] M. G. Moore, O. Zobay, and P. Meystre, Phys. Rev. A **60**, 1491 (1999).
[28] K. Zhang, W. Chen, and P. Meystre, Opt. Commun. **283**, 665 (2009).
[29] J. Larson, B. Damski, G. Morigi, and M. Lewenstein, Phys. Rev. Lett. **100**, 050401 (2008).
[30] J. Larson and M. Lewenstein, New J. Phys. **11**, 063027 (2009).
[31] C. Maschler, H. Ritsch, A. Vukics, and P. Domokos, Opt. Commun. **273**, 446 (2007).
[32] A. Vukics, W. Niedenzu, and H. Ritsch, Phys. Rev. A **79**, 013828 (2009).
[33] B. W. Shore, P. Meystre, and S. Stenholm, J. Opt. Soc. Am. B **8**, 903 (1991).
[34] A. Vukics and P. Domokos, Phys. Rev. A **72**, 031401 (2005).
[35] S. Deachapunya, P. Fagan, A. Major, E. Reiger, H. Ritsch, A. Stefanov, H. Ulbricht, and M. Arndt, Eur. Phys. J. D **46**, 307 (2008).
[36] P. Horak and H. Ritsch, Phys. Rev. A **64**, 033422 (2001).
[37] C. W. Gardiner and P. Zoller, *Quantum Noise*, 2nd ed. (Springer-Verlag, Berlin, 2000).
[38] G. Szirmai, D. Nagy, and P. Domokos, Phys. Rev. A **81**, 043639 (2010).
[39] I. B. Mekhov, C. Maschler, and H. Ritsch, Phys. Rev. Lett. **98**, 100402 (2007).
[40] I. B. Mekhov and H. Ritsch, Phys. Rev. Lett. **102**, 020403 (2009).

[41] J. Dalibard and C. Cohen-Tannoudji, J. Opt. Soc. Am. B **2**, 1707 (1985).
[42] J. Larson and S. Stenholm, Phys. Rev. A **73**, 033805 (2006).
[43] J. Larson, Phys. Scr. **76**, 146 (2007).
[44] P. Horak and H. Ritsch, Phys. Rev. A **55**, 2176 (1997).
[45] C. Cohen-Tannoudji and S. Reynaud, J. Phys. B **10**, 345 (1977).
[46] Y. Castin and J. Dalibard, Europhys. Lett. **14**, 761 (1991).
[47] W. Kohn, Phys. Rev. **115**, 809 (1959).
[48] A. Vukics, C. Maschler, and H. Ritsch, New J. Phys. **9**, 255 (2007).
[49] C. Pethick and H. Smith, *Bose-Einstein Condensation in Dilute Gases* (Cambridge University Press, Cambridge, 2002).
[50] S. Fernández-Vidal, G. De Chiara, J. Larson, and G. Morigi, Phys. Rev. A **81**, 043407 (2010).
[51] A. Vukics and H. Ritsch, Eur. Phys. J. D **44**, 585 (2007).